High-density formation of Ta nanodot induced by remote hydrogen plasma

Yaping Wang[1]*, Daichi Takeuchi[1], Akio Ohta[1, 2], Mitsuhisa Ikeda[1], Katsunori Makihara[1], and Seiichi Miyazaki[1]

[1]*Graduate School of Engineering, Nagoya University, Nagoya 464-8603, Japan*

[2]*Institute for Advanced Research, Nagoya University, Nagoya 464-8603, Japan*

*E-mail: w_yabin@nuee.nagoya-u.ac.jp

We have studied the formation of Ta nanodots (NDs) on thermally grown SiO_2/Si by exposing a thin metal layer to a remote H_2 plasma (H_2-RP) without external heating. Atomic force microscopy (AFM) analyses show that a combination of a Ge (~30.0 nm)/Ta (~2.0 nm) bilayer stack with subsequent H_2-RP exposure is effective for forming electrically isolated Ta NDs with an areal dot density as high as ~10^{11} cm^{-2}, where the Ge layer plays an important role as a barrier layer against the oxidation of the ultrathin Ta layer surface. The change in the chemical structure of the Ge/Ta bilayer stack on SiO_2/Si upon Ta ND formation by H_2-RP exposure is investigated by hard X-ray photoemission spectroscopy (HAXPES) and X-ray photoelectron spectroscopy (XPS).

1. Introduction

The formation of well-controlled metal nanodots (NDs) has been attracting much attention because of their unique physical properties, which enable the improvement of the performance of devices such as floating-gate MOS memories [1-3] and resistive switching devices [4-6]. For resistive random access memory (ReRAM) application, the dispersions of operation voltages were decreased and the ON/OFF current ratio was increased by embedding NDs into dielectric layers, causing electric field concentration [7-9]. Since the resistive switching can be explained by the formation and rupture of conductive filaments in oxide layers as a result of the diffusion of oxygen vacancies, easily oxidized metals such as Ta may be a promising material for NDs embedded in oxide layers. In fact, Ta oxide has been reported as an attractive resistive-switching material because the controllability of the oxygen vacancy concentration in a TaO_x conductive filament leads to superior retention and endurance properties of ReRAMs [10-13]. Various formation techniques of nanodots have been demonstrated over the past decades, such as electron beam lithography followed by etching [14-17], thermal vacuum evaporation using an anodic porous alumina membrane as a template [18-20], and a bio-nanoprocess with the use of a cagelike protein [21-24]. However, these techniques have some drawbacks, for instance, the need to remove unwanted materials and the limited size control of NDs. In order to integrate metal-ND-based devices on the Si platform, ND formation methods should be compatible with the silicon process technology. So far, we have reported the self-assembly formation of metal (Ni, Pt, Pd, and Co) NDs on thermally grown SiO_2 with an areal density as high as ~10^{12} cm^{-2} simply by exposing ultrathin metal films to a remote H_2 plasma (H_2-RP) without external heating [25-28]. This is beneficial for the minimization of metal diffusion into oxide layers, which often degrades the oxide quality and increases leakage current. In this method, the adsorption of atomic hydrogen on a clean metal surface is essential for ND formation due to the local heating caused by the recombination of atomic hydrogen. In practice, when Al films were exposed to H_2-RP, the presence of native oxide on the Al surface significantly

suppresses the rise in surface temperature and prevents ND formation as a consequence [26]. To form NDs made of easily oxidized metal, we proposed to employ amorphous-Ge (a-Ge) films as a capping layer to prevent the oxidation of the metal surface, because a-Ge is completely removed by H_2-RP at an etching rate as high as ~56 nm/min [29]. In this work, we extended our research work to form high-density Ta NDs on SiO_2 by exposing a Ge/Ta bilayer stack to H_2-RP.

2. Experimental procedure

After conventional wet-chemical cleaning steps of a p-type Si(100) substrate with a resistivity of 8.5-11.5 Ω·cm, a ~2.4-nm-thick SiO_2 was thermally grown on the Si substrate by oxidation at 850 ˚C in dry O_2. After that, a ~2.0-nm-thick Ta layer was formed on the ultrathin SiO_2 by electron beam (EB) evaporation at room temperature. Subsequently, a ~30.0-nm-thick Ge layer was deposited on the Ta layer by EB evaporation without air exposure. The Ge/Ta bilayer stack thus prepared was exposed simply to H_2-RP without external heating. The plasma was generated by inductive coupling with an external single-turn antenna connected to a 60 MHz generator through a matching circuit. During H_2-RP exposure, the gas pressure and very high frequency (VHF) power were maintained at 13.3 Pa and 500 W, respectively. The parameter in this work is exposure time. To evaluate the effect of the Ge capping layer, a ~ 2.0-nm-thick Ta single layer deposited on SiO_2 was also exposed to H_2-RP for comparison.

The change in the surface morphology and the formation of the Ta NDs were evaluated by atomic force microscopy (AFM). The impact of H_2-RP exposure on the chemical structure of Ge/Ta bilayer stacks on a ~2.4-nm-thick SiO_2/Si substrate was investigated by X-ray photoelectron spectroscopy (XPS) under monochromatized Al Kα radiation (hν = 1486.6eV) and hard X-ray photoemission spectroscopy (HAXPES) under synchrotron radiation (hν = 7939eV) at beam line BL47XU of SPring-8. Because of the detection limit of HAXPES in the depth direction being as deep as ~30 nm from the surface, we can discuss the chemical

bonding features of the Ta layer through the Ge capping layer from core-line signals such as Ta $3d_{5/2}$ and Ge $2p_{3/2}$ spectra. XPS enables us to perform surface-sensitive measurements in comparison with the HAXPES.

3. Results and discussion

Figure 1 shows AFM topographic images of the Ge/Ta bilayer stack and the Ta single layer formed on the SiO_2/Si(100) substrate taken before and after H_2-RP exposure. An AFM image of the Ge/Ta bilayer taken prior to the H_2-RP exposure shows a fairly smooth surface morphology with the root-mean-square (RMS) roughness of 0.24 nm as shown in Fig. 1(a). Figure 1(c) shows no difference from the surface morphology of the predeposition Ta layer. This result indicates uniform surface coverage by the Ge layer. By exposing the Ge/Ta bilayer on SiO_2 to H_2-RP, the RMS roughness is increased by a factor of ~2.4 and the formation of NDs with an areal density as high as $\sim 7.1\times10^{11}$ cm^{-2} is observed, as shown in Fig. 1(b). The etching of the Ge layer by H_2-RP exposure is also detected from the results of the HAXPES and XPS analyses, as will be discussed later. These results indicate that the H_2-RP exposure promoted the cohesive action of Ta atoms on the SiO_2 surface after the etching of the Ge layer. On the other hand, no significant change in the RMS roughness for the sample with only the Ta single layer is detected after the H_2-RP exposure under the same conditions, as shown in Fig. 1(d), which can be interpreted to mean that the presence of native oxide on the Ta surface suppresses the rise in surface temperature and prevents ND formation, as similarly seen in the case of Al [9]. The size distribution of the Ta NDs is evaluated from the cross-sectional profile of the AFM image and is shown by the histogram in Fig. 2. The obtained histogram of the Ta ND height shows a lognormal distribution with a full width at half maximum (FWHM) of ~1.2 nm; the average height of the Ta ND was found to be ~2.3 nm.

To confirm electrical isolation among the NDs, topographic and the corresponding surface potential images were simultaneously taken by an AFM/Kelvin probe technique by scanning

the sample surface with an electrically biased AFM tip in the tapping mode, as shown in Fig. 3. Without any bias applied to the sample surface, a uniform surface potential image is observed [Fig. 3(a)]. Immediately after the sample surface was scanned over a region 500 × 500 nm^2 in size with an AFM tip biased at -4.0 V with respect to the Si substrate, the surface potential decreased by 30 mV in the scanned area [Fig. 3(b)]. On the other hand, no change is detected in the surface potential in the unbiased area. In contrast, prior to the H_2-RP exposure of the sample, no change in the surface potential is confirmed after applying tip biases because of the highly electrically conductive surface. These results indicate electron injection from the Rh-coated AFM tip to the Ta NDs and stable electron storage in the Ta NDs. In addition, upon scanning the surface with a tip biased at +4.0 V, the surface potential rose by 35 mV, indicating electron extraction from the Ta NDs [Fig. 3(c)]. These results indicate the formation of electrically isolated Ta NDs.

The impact of H_2-RP exposure on the chemical bonding features of the Ge/Ta bilayer stack on the SiO_2/Si substrate is evaluated by HAXPES and XPS measurements. Ta $3d_{5/2}$ and Ge $2p_{3/2}$ core-line spectra taken for the Ge/Ta bilayer on SiO_2/Si before and after H_2-RP exposure for 1 min were measured by HAXPES and are shown in Figs. 4(a) and 4(b), respectively. In each spectrum, the photoelectron take-off angle was set at 87º. Ta $3d_{5/2}$ signals from the sample before H_2-RP exposure indicate the Ta-Ta bonding units due to the metallic Ta component, which indicates that the surface oxidation of the Ta layer is effectively suppressed by the deposition of the ~30.0-nm-thick Ge capping layer. After H_2-RP exposure, metallic Ta $3d_{5/2}$ signals from Ta NDs are clearly observed without any peak energy shift compared with the signals before H_2-RP exposure. In addition, an increase in the intensity of the Ta $3d_{5/2}$ signals originating from Ta oxide can be explained by the surface oxidation of Ta NDs by air exposure. The intensity of Ge $2p_{3/2}$ signals originating from the capping layer is markedly decreased and slightly shifted toward the lower binding energy side by about 0.2 eV compared with those before H_2-RP exposure. This observed energy shift of Ge $2p_{3/2}$ signals can be explained by the incorporation of less electronegative Ta ions

(χ_{Ta} = 1.50) into the Ge-Ge network as the second nearest neighbors of the Ge atoms (χ_{Ge} = 2.01) [30]. These results indicate that the etching of the Ge layer and the incorporation of Ge atoms into the Ta layer proceed during H_2-RP exposure. This Ge incorporation into the Ta layer is also confirmed from the depth profiling of the chemical structure evaluated using the photoelectron-take-off angle dependence of Ge $2p_{3/2}$ and Ta $3d_{5/2}$ core-line signals. Moreover, the lack of any change in the spectral shape of the SiO_2 component upon H_2-RP exposure was also confirmed from the Si 1s signals (data not shown), which implies that the amounts of diffused and incorporated Ta and Ge atoms from the Ge/Ta bilayer into the SiO_2 layer upon H_2-RP exposure are quite small and within the detection limit of HAXPES (<0.1 at.%). Figure 5 shows the change in the integrated intensity of Ge $2p_{3/2}$ signals with H_2-RP exposure time. With increasing H_2-RP exposure time, the Ge $2p_{3/2}$ signal intensity is found to markedly decrease owing to the etching of the Ge layer. The remaining Ge thickness is roughly calculated from the integrated intensity ratio of Ge $2p_{3/2}$ signals from the Ge layer to Ta $3d_{5/2}$ or Ta $4f_{7/2}$ signals from the Ta layer or Ta NDs in consideration of the escape depth and the photoionized cross section for each photoelectron. As a result, after H_2-RP exposure for 1 min, the remaining Ge thickness was considerably decreased to ~1.5 nm. With further increase in the H_2-RP exposure time to over 3 min, the remaining Ge thickness was estimated to be less than ~0.1 nm.

Finally, the formation of high-density Ta NDs by H_2-RP exposure on the Ge/Ta bilayer stack on the SiO_2/Si substrate is summarized in the schematic illustration shown in Fig. 6. In the early stage of H_2-RP exposure [as shown in Fig. 6(b)], the etching of Ge proceeds and a small amount of Ge is incorporated into the Ta layer. Then, the atomic hydrogen adsorbed on the Ta(Ge) surface can combine to form hydrogen molecules, resulting in local heating at the surface, which induces the surface migration and agglomeration of Ta atoms with the desorption of Ge [as shown in Fig. 6(c)]. After that, a high density of Ta NDs are formed and the surface is oxidized by air exposure [as shown in Fig. 6(d)]. The presence of the Ge capping layer as a barrier layer against the oxidation of the Ta surface is the key to the

formation of a high density of Ta NDs by H_2-RP exposure. This technique is promising for the ND formation of easily oxidized metals.

4. Conclusions

We demonstrated a novel technique for the formation of Ta NDs with an areal density as high as ~10^{11} cm^{-2} by exposing a Ge/ultrathin Ta bilayer stack on thermally grown SiO_2 to H_2-RP without external heating. The electrical isolation among the Ta NDs was confirmed by an AFM/Kelvin probe technique. XPS results indicated that the etching of the Ge layer by H_2-RP exposure was accompanied by the agglomeration of Ta atoms on the SiO_2 surface caused by local heating associated with the recombination of atomic hydrogen.

Acknowledgments

Part of this work was performed at the Venture Business Laboratory, Nagoya University, Japan. The HAXPES experiments were carried out at BL47XU in SPring-8 with the approval of JASRI as a Nanotechnology Support Project of the Ministry of Education, Culture, Sports, Science, and Technology (Proposals No. 2014B0109/BL47XU and 2015A0109/BL47XU). We would like to thank Dr. E. Ikenaga (JASRI) for fruitful discussion and assistance in the experiments.

References

1. Y. Pei, C. Yin, T. Kojima, M. Nishijima, T. Fukushima, T. Tanaka, and M. Koyanagi, Appl. Phys. Lett. **95**, 033118 (2009).
2. K. Yamada, S. Yoshii, S. Kumagai, A. Miura, Y. Uraoka, T. Fuyuki, and I. Yamashita, Jpn. J. Appl. Phys. **45**, 8946 (2006).
3. Z. Liu, C. Lee, V. Narayanan, G. Pei, and E. C. Kan, IEEE Trans. Electron Devices **49,** 1606 (2002).
4. J. H. Yoon, K. M. Kim, M. H. Lee, S. K. Kim, G. H. Kim, S. J. Song, J. Y. Seok, and C. S. Hwang, Appl. Phys. Lett. **97**, 232904 (2010).
5. J. Choi, A. C. Torrezan, K. J. Norris, F. Miao, J. P. Strachan, M. Zhang, D. A. A. Ohlberg, N. P. Kobayashi, J. J. Yang, and R. S. Williams, Nano Lett. **13**, 3213 (2013).
6. A. J. Choi, A. B. K. Chen, X. Yang, and I. Chen, Adv. Mater. **23**, 3847 (2011).
7. M. Uenuma, K. Kawano, B. Zheng, N. Okamoto, M. Horita, S. Yoshii, I. Yamashita, and Y. Uraoka, Nanotechnology **22**, 215201(2011).
8. W. Banerjee, S. Maikap, S. Z. Rahaman, A. Prakash, T. C. Tien, W. C. Li, and J. R. Yang, J. Electrochem. Soc. **159**, H177 (2012).
9. W. Guan, S. Long, R. Jia, and M. Liu, Appl. Phys. Lett. **91**, 062111 (2007).
10. T. Ninomiya, Z. Wei, S. Muraoka, R. Yasuhara, K. Katayama, and T. Takagi, IEEE Trans. Electron Devices **60**, 1384 (2013).
11. Q. Wang, Y. Itoh, T. Tsuruoka, S. Ohtsuka, T. Shimizu, S. Shingubara, T. Hasegawa, and M. Aono, Phys. Status Solidi: Rapid Res. Lett. **9**, 166 (2015).
12. B. Xiao and S. Watanabe, Nanoscale **6**, 10169 (2014).
13. A. J. Lohn, J. E. Stevens, P. R. Mickel, D. R. Hughart, and M. J. Marinella, ECS Trans. **58** [5], 59 (2013).
14. Y. Lin, Y. Zou, Y. Mo, J. Guo, and R. G. Lindquist, Sensors **10**, 9397 (2010).
15. A. A. Tseng, K. Chen, C. D. Chen, and K. J. Ma, IEEE Trans. Electron. Packag. Manuf. **26** (2003).

16. A. Chen, S. J. Chua, P. Chen, X. Y. Chen, and L. K. Jian, Nanotechnology **17**, 15 (2006).
17. J. Stodolka, D. Nau, M. Frommberger, C. Zanke, H. Giessen, and E. Quandt, Microelectron. Eng. **78-79**, 442 (2005).
18. S. K. Park, J. S. Noh, W. B. Chin, and D. D. Sung, Curr. Appl. Phys. **7**, 180 (2007).
19. S. Shingubara, J. Nanopart. Res. **5**, 17 (2003).
20. H. Masuda and M. Satoh, Jpn. J. Appl. Phys. **35**, L126 (1996).
21. T. Hikono, Y. Uraoka, T. Fuyuki, and I. Yamashita, Jpn. J. Appl. Phys. **42**, L398 (2003).
22. M. Allen, D. Willits, J. Mosolf, M. Young, and T. Douglas, Adv. Mater. **14**, 1562 (2002).
23. I. Yamashita, Thin Solid Films **393**, 12 (2001).
24. Y. Nakama, J. Ohta, and M. Nunoshita, Jpn. J. Appl. Phys. **47**, 3028 (2008).
25. K. Makihara, K. Shimanoe, M. Ikeda, S. Higashi, and S. Miyazaki, Jpn. J. Appl. Phys. **47**, 3099 (2008).
26. K. Makihara, K. Shimanoe, A. Kawanami, M. Ikeda, S. Higashi, and S. Miyazaki, J. Opt. Adv. Mater. **12**, 626 (2010).
27. K. Shimanoe, K. Makihara, M. Ikeda, and S. Miyazaki, IEICE Trans. Electron. **E92-C**, 616 (2009).
28. A. Kawanami, K. Makihara, M. Ikeda, and S. Miyazaki, Jpn. J. Appl. Phys. **49**, 08JA04K (2010).
29. K. Makihara, M. Ikeda, T. Okada, and S. Miyazaki, Jpn. J. Appl. Phys. **53**, 11RA02 (2014).
30. L. Pauling, *The Nature of Chemical Bond* (Cornell University Press, Ithaka, NY, 1960) 3rd ed.

Figure Captions

Fig. 1. (Color online) AFM topographic images of (a, b) Ge (~30 nm)/Ta (~2 nm)/SiO_2 and (c, d) Ta (~2 nm)/SiO_2 taken (a, c) before and (b, d) after H_2-RP exposure for 10 min.

Fig. 2. (Color online) Distribution of Ta ND heights obtained from AFM image shown in Fig. 1(b). The solid line denotes the lognormal function well fitted to the measured distribution.

Fig. 3. (Color online) Surface potential images of Ta NDs measured (a) before and after electron injection and extraction at tip biases of (b) –4.0 V and (c) +4.0 V, respectively. The surface potential was measured in a noncontact Kelvin probe mode after tapping the sample surface with an electrically biased AFM tip coated with Rh.

Fig. 4. (Color online) (a) Ta $3d_{5/2}$ and (b) Ge $2p_{3/2}$ spectra for the Ge/Ta bilayer stack on the SiO_2/Si before and after H_2-RP exposure. In these spectra, Ta $3d_{5/2}$ and Ge $2p_{3/2}$ photoelectron intensities for the sample before H_2-RP exposure are shown at half and 60 times the actual values, respectively.

Fig. 5. (Color online) Change in the integrated intensity of Ge $2p_{3/2}$ core-line with H_2-RP exposure time. The photoelectron take-off angles in HAXPES and XPS were set at 87 and 90º, respectively. In the figure, the remaining Ge thickness is roughly calculated from the integrated intensity ratio of Ge $2p_{3/2}$ signals to Ta $3d_{5/2}$ or Ta $4f_{7/2}$ signals.

Fig. 6. (Color online) Schematic views of the sample structure at each process step of Ta ND formation by exposing Ge/Ta bilayer stack to H_2-RP. Ge/Ta bilayer stack on SiO_2/Si (a) before H_2-RP exposure, (b) in the early stage of H_2-RP exposure, (c) in the middle stage of

H_2-RP exposure [after the Ta (Ge) surface was revealed], and (d) after H_2-RP exposure (Ta ND formation).

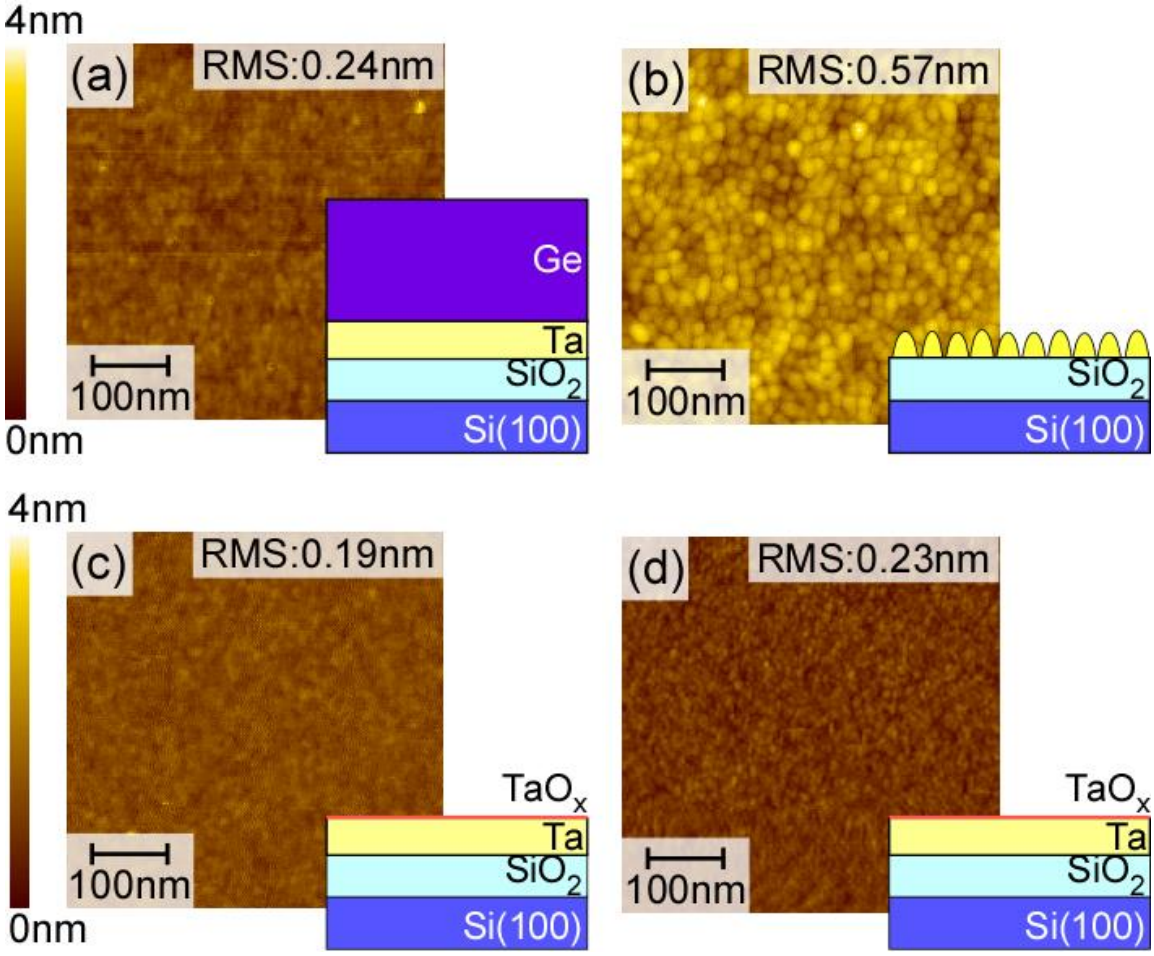
4nm
(a)
RMS:0.24nm
Ge
Ta
SiO2
Si(100)
100nm
0nm
(b)
RMS:0.57nm
SiO2
Si(100)
100nm
4nm
(c)
RMS:0.19nm
TaOx
Ta
SiO2
Si(100)
100nm
0nm
(d)
RMS:0.23nm
TaOx
Ta
SiO2
Si(100)
100nm

Fig. 1

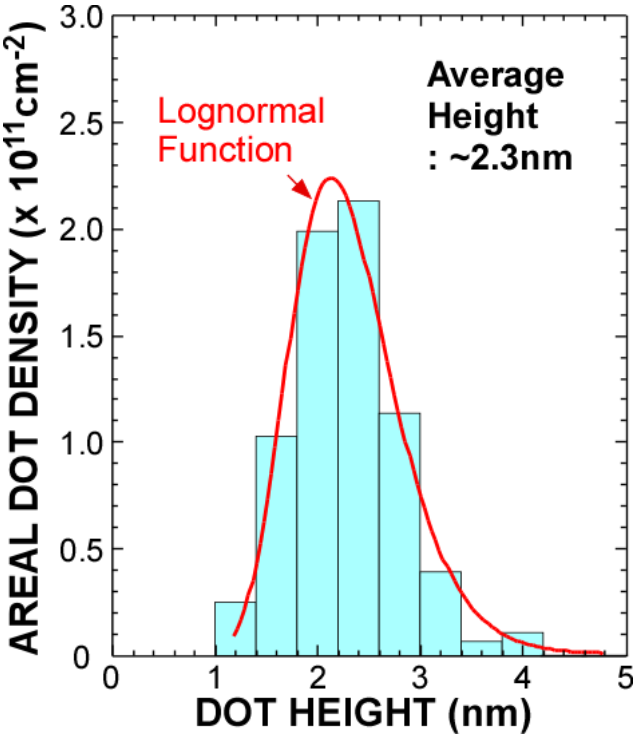
AREAL DOT DENSITY (x 10^11 cm^-2)
DOT HEIGHT (nm)
Lognormal Function
Average Height : ~2.3nm
0
0.5
1.0
1.5
2.0
2.5
3.0
0
1
2
3
4
5

Fig. 2

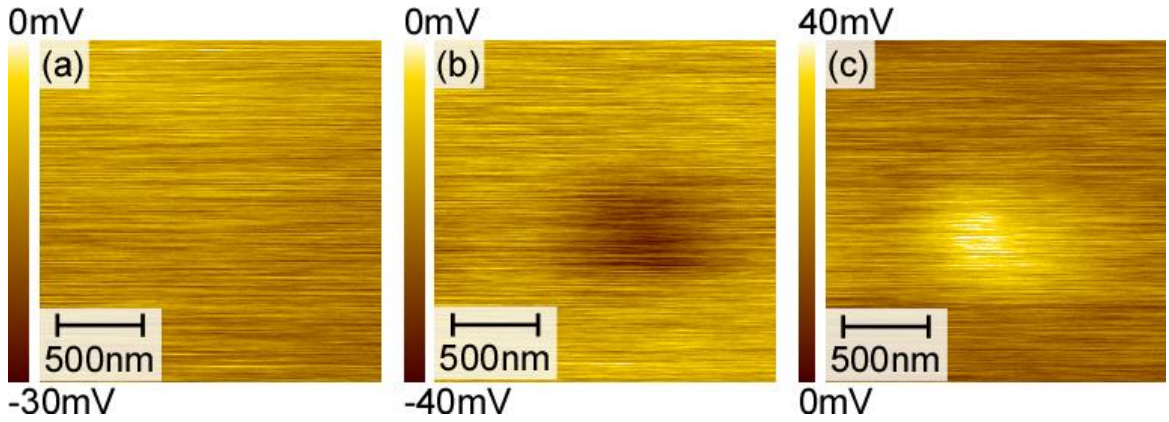

Fig. 3

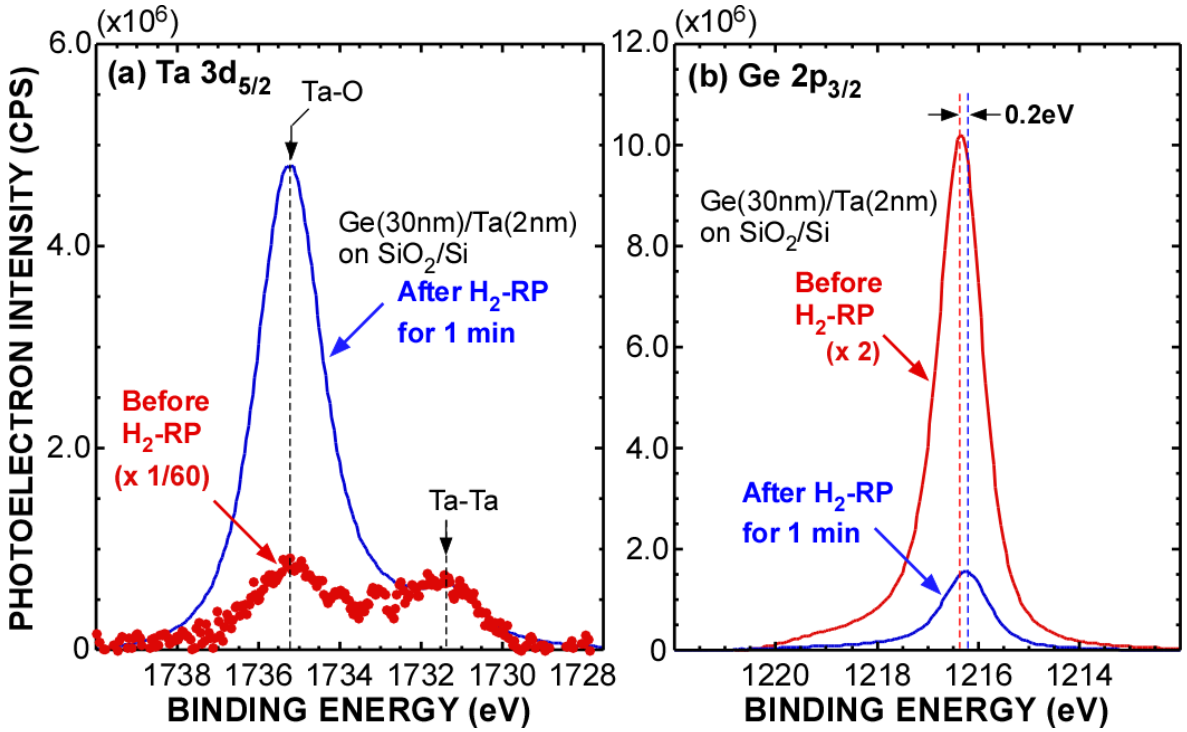
(x10^6)
6.0
4.0
2.0
0
PHOTOELECTRON INTENSITY (CPS)
(a) Ta 3d5/2
Ta-O
Ge(30nm)/Ta(2nm)
on SiO2/Si
After H2-RP
for 1 min
Before
H2-RP
(x 1/60)
Ta-Ta
1738 1736 1734 1732 1730 1728
BINDING ENERGY (eV)
(x10^6)
12.0
10.0
8.0
6.0
4.0
2.0
0
(b) Ge 2p3/2
0.2eV
Ge(30nm)/Ta(2nm)
on SiO2/Si
Before
H2-RP
(x 2)
After H2-RP
for 1 min
1220 1218 1216 1214
BINDING ENERGY (eV)

Fig. 4

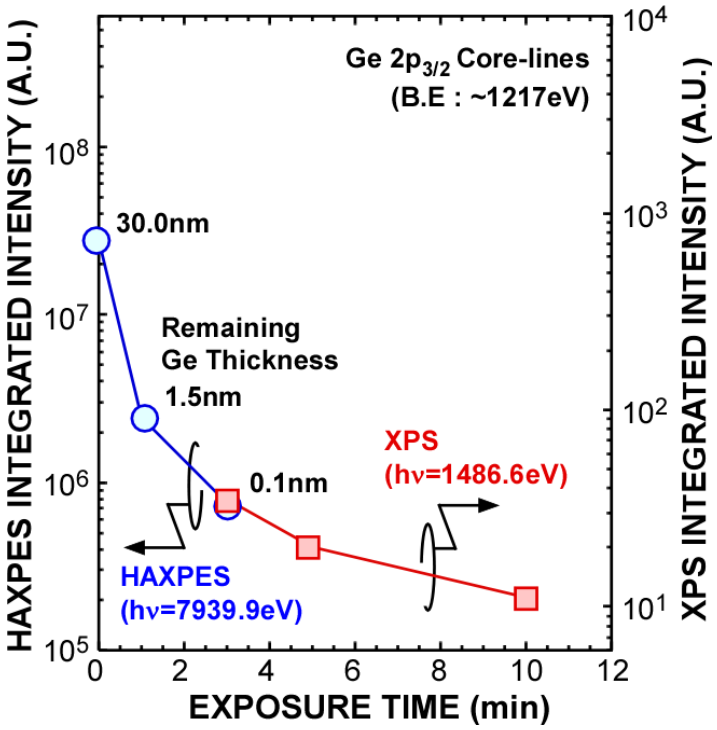
Ge 2p3/2 Core-lines
(B.E : ~1217eV)
30.0nm
Remaining
Ge Thickness
1.5nm
0.1nm
XPS
(hν=1486.6eV)
HAXPES
(hν=7939.9eV)
HAXPES INTEGRATED INTENSITY (A.U.)
XPS INTEGRATED INTENSITY (A.U.)
EXPOSURE TIME (min)
10^8
10^7
10^6
10^5
10^4
10^3
10^2
10^1
0
2
4
6
8
10
12

Fig. 5

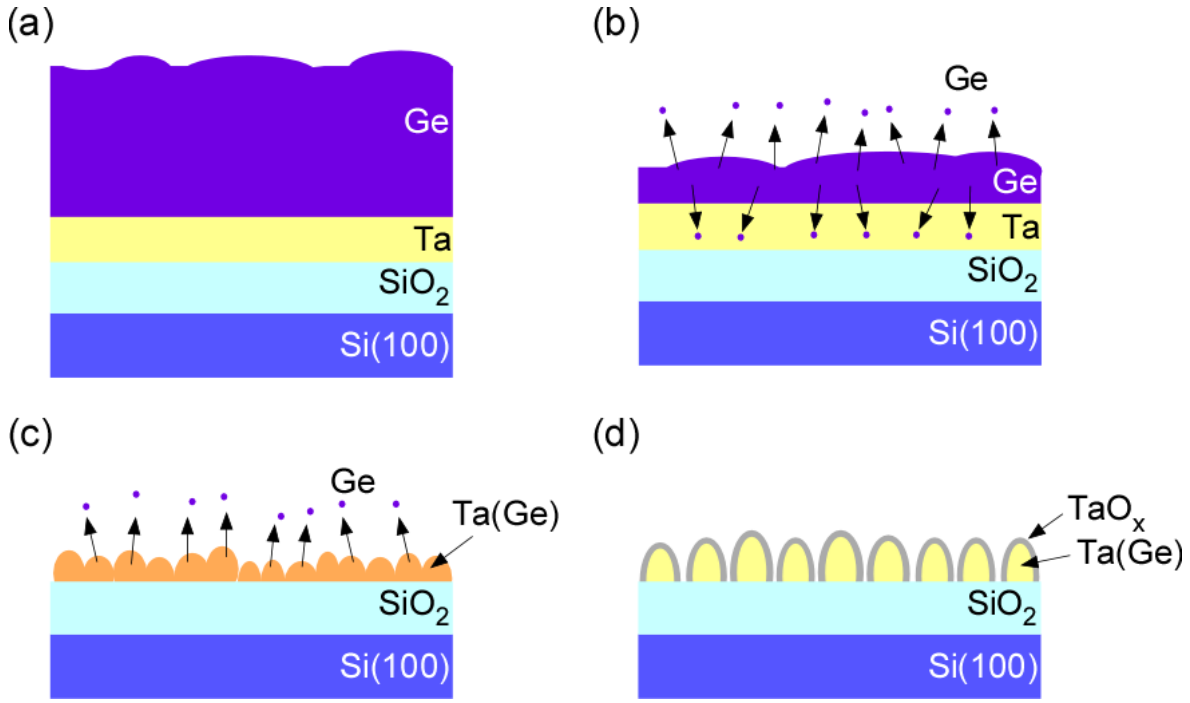
(a)
Ge
Ta
SiO2
Si(100)
(b)
Ge
Ge
Ta
SiO2
Si(100)
(c)
Ge
Ta(Ge)
SiO2
Si(100)
(d)
TaOx
Ta(Ge)
SiO2
Si(100)

Fig. 6